Orbital Properties of $Sr_3Ru_2O_7$ and Related Ruthenates Probed by ^{17}O-NMR

K. Kitagawa,[1] K. Ishida,[1,2] R. S. Perry,[1,2,3] H. Murakawa,[1] K. Yoshimura,[4] and Y. Maeno[1,2]

[1]*Department of Physics, Graduate School of Science, Kyoto University, Kyoto 606-8502, Japan**
[2]*Kyoto University International Innovation Center, Kyoto 606-8501, Japan*
[3]*School of Physics and Astronomy, University of St. Andrews, Fife KY16 9SS, Scotland*
[4]*Department of Chemistry, Graduate School of Science, Kyoto University, Kyoto 606-8502, Japan*

(Dated: February 6, 2008)

We report a site-separated ^{17}O-NMR study of the layered perovskite ruthenate $Sr_3Ru_2O_7$, which exhibits nearly two-dimensional transport properties and itinerant metamagnetism at low temperatures. The local hole occupancies and the spin densities in the oxygen $2p$ orbitals are obtained by means of tight-binding analyses of electric field gradients and anisotropic Knight shifts. These quantities are compared with two other layered perovskite ruthenates: the two-dimensional paramagnet Sr_2RuO_4 and the three-dimensional ferromagnet $SrRuO_3$. The hole occupancies at the oxygen sites are very large, about one hole per ruthenium atom. This is due to the strong covalent character of the Ru-O bonding in this compound. The magnitude of the hole occupancy might be related to the rotation or tilt of the RuO_6 octahedra. The spin densities at the oxygen sites are also large, 20-40% of the bulk susceptibilities, but in contrast to the hole occupancies, the spin densities strongly depend on the dimensionality. This result suggests that the density-of-states at the oxygen sites plays an essential role for the understanding of the complex magnetism found in the layered perovskite ruthenates.

PACS numbers: 76.60.-k,74.70.Pq,73.43.Nq

I. INTRODUCTION

The Ruddlesden-Popper (R-P) series of layered perovskite ruthenates has attracted great interest because of their wide variety of phenomena. The strontium ruthenates $Sr_{n+1}Ru_nO_{3n+1}$ are metallic members of the R-P perovskite ruthenates featuring various kinds of itinerant magnetism and magnetic fluctuations. The two-dimensional member ($n = 1$) Sr_2RuO_4 is paramagnetic and exhibits unconventional superconductivity attributable to p-wave pairing,[1,2,3] originating from electron correlations in the Ru $4d_{xy}$ band. At the same time, it possesses strong incommensurate antiferromagnetic fluctuations[4] due to nesting of the $4d_{yz,zx}$ bands. The three-dimensional end member ($n = \infty$) $SrRuO_3$ is an itinerant ferromagnet with a Curie temperature of 160 K.[5]

The intermediate dimensional, bilayer member ($n = 2$) $Sr_3Ru_2O_7$ does not exhibit magnetic order at zero magnetic field and ambient pressure. Nevertheless, $Sr_3Ru_2O_7$ is considered to be very close to a ferromagnetic instability: (a) the uniform susceptibility has a peak around 16 K, (b) the Wilson ratio is quite large ~ 10, and (c) along c-axis applying small uniaxial pressure of about 0.1 GPa pushes $Sr_3Ru_2O_7$ into a ferromagnetic phase below 80 K.[6,7] At ambient pressure, field-induced metamagnetic transitions are observed.[8,9] The investigation of those metamagnetic transitions leads to a phase diagram with a line of first-order phase transitions terminating at a critical end point. Furthermore, the critical end temperature T^* is extremely low: $T^* = 1.2$ K for $H \perp c$ and T^* vanishes for $H \parallel c$.[10] In the latter case ($H \parallel c$), the existence of a metamagnetic quantum critical point (MMQCP) was proposed.[11,12] In our previous ^{17}O-NMR study with $H \parallel c$, we reported the measurement of the nuclear spin-lattice relaxation rate $1/T_1$, which probes the spin fluctuations, and concluded that two-dimensional ferromagnetic character is dominant at high temperatures. In contrast, non-ferromagnetic (mostly incommensurate antiferromagnetic) fluctuations diverge for $T \to 0$ K near the MMQCP.[13]

Such competitions between itinerant ferromagnetism and incommensurate antiferromagnetism in $Sr_{n+1}Ru_nO_{3n+1}$ are a result of the existence of narrow bands and a high density-of-states (DOS) at the Fermi level E_F created by ruthenium $4d$ and oxygen $2p$ orbitals. According to a band-structure calculation for Sr_2RuO_4,[14] $4d$-$2p$ antibonding bands at the Fermi level create 18% of the DOS in the oxygen $2p$ orbitals and possibly play a crucial role for the electronic and/or structural instabilities. The large DOS at the oxygen sites is unlikely for $3d$ transition-metal oxides because the covalency between the d and $2p$ orbitals is usually rather weak. Our concerns are: (i) How does the hole occupancy or DOS in the oxygen $2p$ orbitals affect the occurrence of itinerant ferromagnetism or antiferromagnetism and (ii) what is the relationship between dimensionality and magnetism.

In this article, we report a detailed site-separated ^{17}O-NMR study of $Sr_3Ru_2O_7$. In Sec. III B, we estimate the hole occupancies in the $2p$ orbitals from the NMR quadrupole splittings at the oxygen sites. Since the oxygen $2p$ orbitals feature a magnetic-dipole type of hyperfine interaction, the anisotropy of the Knight shifts needs to be considered. In Sec. III C we obtain the spin susceptibility of each orbital at all oxygen sites from the Knight shifts. For comparison, we also analyze the related ruthenates Sr_2RuO_4 and $SrRuO_3$ applying the same method.

II. EXPERIMENT

In our NMR experiment we used singe crystals of $Sr_3Ru_2O_7$ which were grown in a floating-zone image furnace.[15] We exchanged natural oxygen ^{16}O ($I = 0$) for ^{17}O ($I = 5/2$). The substitution was performed in a silica-glass-tube furnace, where the samples were kept for one week at 1050°C in a 70% concentrated $^{17}O_2$ atmosphere. Although the gain of mass, estimated to be 0.9%, could not be observed, the measured ^{17}O-NMR signals assure that the isotope substitution process was successful at least over the penetration depth accessible in our experiment, *i. e.* several micro meters. This is sufficient to ignore surface related effects. After the annealing process, we confirmed the residual in-plane resistivity, to be 0.8 $\mu\Omega$·cm. This is enough clean to observe the intrinsic behavior of this system.[16]

Great care was taken to keep the orientation of the sample throughout the field-dependent measurements. For this purpose, complex rf components were introduced outside the cryostat. This ensured that the measurements for all desired field strengths, corresponding to frequencies of 10-80 MHz, could be carried out using only one probing coil. A homemade wide-band pre-amplifier designed with high-electron-mobility transistors was immersed in liquid nitrogen to obtain an excellent noise figure of 0.5 dB. Furthermore it had a short dead-time of less than 3 μs after saturation. With this setup it was possible to overcome the issues of the weak intensities of signals and shortness of NMR decoherence times.

III. RESULTS AND DISCUSSIONS

A. NMR spectra and site-assignment

^{17}O-NMR lines can be described using anisotropic Knight shifts and the quadrupole interaction perturbation of the electric field gradients (EFG). For each site, the resonance field $H_{\rm res}$ corresponding to the $m \leftrightarrow m-1$ resonance can be approximately written as[19,42]

$$\frac{H_0 - H_{\rm res}}{H_{\rm res}} = {}^{17}K^{\rm iso} + \left\{ \frac{1}{2}\frac{{}^{17}\nu_{\rm Q}\left(m-\frac{1}{2}\right)}{{}^{17}\gamma H_{\rm res}} + \frac{1}{2}{}^{17}K^{\rm ax} \right\}(3\cos^2\theta - 1) - \frac{1}{2}\left\{ {}^{17}K^{\rm aniso,\perp} + \left(m-\frac{1}{2}\right)\frac{{}^{17}\nu_{\rm Q}}{{}^{17}\gamma H_{\rm res}}\eta \right\}\sin^2\theta\cos 2\phi, \quad (1)$$

where (θ, ϕ) are Euler's coordinates with respect to the largest principal axis of the diagonalized EFG, and $^{17}\gamma$ (= 5.7719 MHz/T) is the gyromagnetic ratio of an ^{17}O nucleus. H_0 is the resonance field of a free ^{17}O atom at the resonance frequency $^{17}\gamma H_0$. $^{17}K^{\rm iso}$ is the isotropic Knight shift, $^{17}K^{\rm ax}$ is the axial anisotropic shift, and $^{17}K^{\rm aniso,\perp}$ is the in-plane anisotropic shift perpendicular to the principal axis for lower symmetric sites. $^{17}\nu_{\rm Q}$ is the pure quadrupole frequency and $\eta\,(0 \le \eta \le 1)$ is the asymmetric parameter of the EFG.

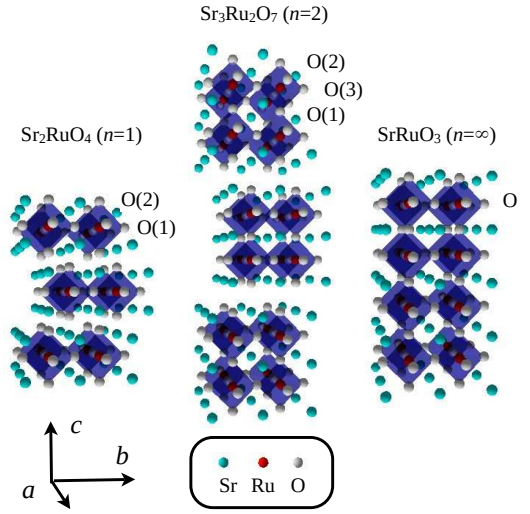

FIG. 1: (color online). Crystal structure of the Ruddlesden-Popper series $Sr_{n+1}Ru_nO_{3n+1}$ for Sr_2RuO_4 ($n = 1$, left), $Sr_3Ru_2O_7$ ($n = 2$, middle), and $SrRuO_3$ ($n = \infty$, right). The axes a and b are taken along a Ru-O-Ru bonding. For $Sr_3Ru_2O_7$ and $SrRuO_3$, symmetries are reduced because of a rotation and a tilt of the RuO_6 octahedra, respectively.[17,18] For simplicity, these effects are not shown. There are apical O(2) and in-plane O(1) sites in Sr_2RuO_4. $Sr_3Ru_2O_7$ has two kinds of apical sites. For $Sr_3Ru_2O_7$, we label the inner-apical, outer-apical, and in-plane sites O(1), O(2), and O(3) sites, respectively.

Crystallographically, three inequivalent oxygen sites exist in the bilayered perovskite structure (Fig. 1). More-

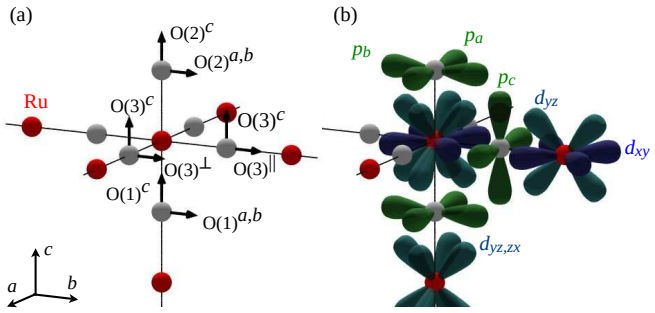

FIG. 2: (color online). (a) ^{17}O-NMR spectral site notations for $Sr_3Ru_2O_7$. Arrows denote the corresponding field directions, $H \parallel c$ and $H \parallel [100]$. (b) Relevant atomic orbitals at the Fermi surfaces for $Sr_3Ru_2O_7$. We treat interactions of electrons with nuclei by a method of linear combination of atomic orbitals, namely the tight-binding method. Ru^{4+} ions realize a low-spin configuration and the resulting t_{2g} ($= 4d_{xy}, 4d_{yz}, 4d_{zx}$) orbitals hybridize with the oxygen $2p_\pi$ ($= 2p_x, 2p_y, 2p_z$) orbitals.

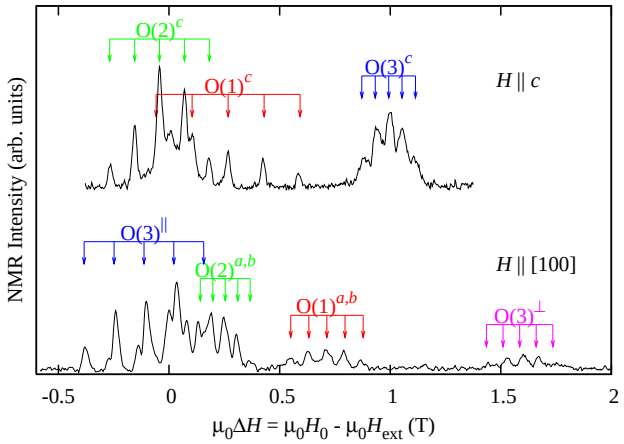

FIG. 3: (color online). Field-swept ^{17}O-NMR spectra for $Sr_3Ru_2O_7$ with a frequency of 72.5 MHz at 1.7 K. The corresponding ^{17}O-NMR field for a free atom, $\mu_0 H_0$, is 12.56 T. $H_{\rm ext}$ is the external applied field. Lines from each site must consist of five resonances due to the perturbations from the electric quadrupole interaction. The unassigned sites, which exhibit a smaller sample-dependent intensity, are attributed to an impurity phase of Sr_2RuO_4.

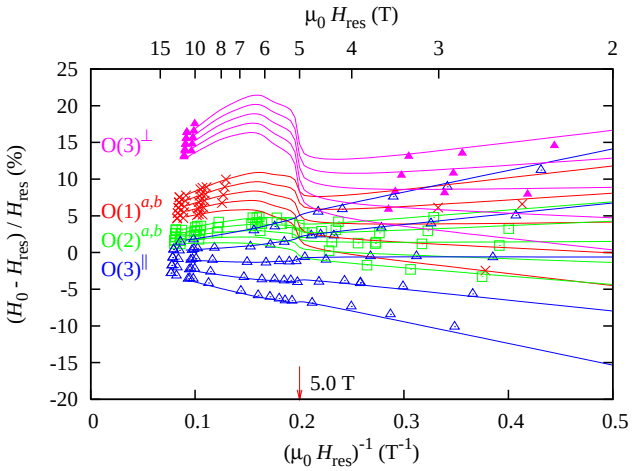

FIG. 4: (color online). NMR spectral positions as a function of $H_{\rm res}^{-1}$ for $Sr_3Ru_2O_7$ with $H \parallel [100]$. All data points are taken from the field-swept spectra at 1.7 K. The arrow denotes the metamagnetic field. At and slightly below the metamagnetic field high transverse relaxation rates $1/T_2$ prevent observations of signals from the O(1) and O(3)$^\perp$ sites. The plotted lines are based on eq. (1). The values of EFGs are listed in Sec. III B. The Knight shifts are evaluated in Sec. III C.

over, when a field is applied perpendicular to the c axis, the in-plane site O(3) splits into two configurations, O(3)$^\parallel$ and O(3)$^\perp$, as shown in Fig. 2(a). Figure 3 shows a typical ^{17}O-NMR spectra for $Sr_3Ru_2O_7$.

For the apical sites (O(1) and O(2) in $Sr_3Ru_2O_7$) one can rewrite the parameters as follows:

$$
\begin{aligned}
{}^{17}K^{\rm iso} &= \frac{1}{3}({}^{17}K^{c}_{\rm obs} + 2\,{}^{17}K^{a,b}_{\rm obs}),\\
{}^{17}K^{\rm ax} &= {}^{17}K^{c}_{\rm obs} - {}^{17}K^{\rm iso}\\
&= \frac{2}{3}({}^{17}K^{c}_{\rm obs} - {}^{17}K^{a,b}_{\rm obs}),\\
{}^{17}K^{{\rm aniso},\perp} &= 0,\\
{}^{17}\nu_{\rm Q} = {}^{17}\nu^{c} &= -2\,{}^{17}\nu^{a,b},\\
\eta &= 0.
\end{aligned}
$$

Here, $^{17}K^{i}_{\rm obs}$ is the observed Knight shift for direction i.

For in-plane sites (O(3) for $Sr_3Ru_2O_7$) the parameters are:

$$
\begin{aligned}
{}^{17}K^{\rm iso} &= \frac{1}{3}({}^{17}K^{\parallel}_{\rm obs} + {}^{17}K^{\perp}_{\rm obs} + {}^{17}K^{c}_{\rm obs}),\\
{}^{17}K^{\rm ax} &= {}^{17}K^{\parallel}_{\rm obs} - {}^{17}K^{\rm iso},\\
{}^{17}K^{{\rm aniso},\perp} &= {}^{17}K^{\perp}_{\rm obs} - {}^{17}K^{c}_{\rm obs},\\
{}^{17}\nu_{\rm Q} &= {}^{17}\nu^{\parallel}.
\end{aligned}
$$

From eq. (1), we expect a linear relationship between $(H_0 - H_{\rm res})/H_{\rm res}$ and $(H_{\rm res})^{-1}$ as long as the magnetization M is linear with H. Figure 4 displays such a behavior for $H \parallel [100]$ (see Ref. 20 for $H \parallel c$). The linear relationships are realized much below and above the metamagnetic field $H_{\rm M}$. The plot is helpful to group

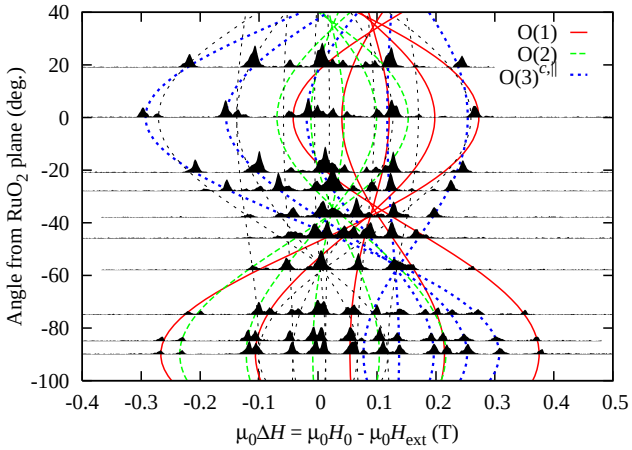

FIG. 5: (color online). Field-swept NMR spectra with various field orientations for $Sr_3Ru_2O_7$ at 1.7 K with a frequency of 21.3 MHz, i. e. $\mu_0 H_0 \sim 3.7$ T. The orientation is varied from [100] (0 deg. in the plot) to the c axis ($\pm$90 deg.) by the use of a backlash-free rotator in an 8 T split-coil magnet. All curves are drawn in the same scheme as in Fig. 4. The O(3)$^\perp$ lines are not observable in this configuration due to a high transverse relaxation rate $1/T_2$. The narrow dotted curves, which are not attributable to $Sr_3Ru_2O_7$, originate from the Sr_2RuO_4-O(1) site in the impurity phase.

spectral lines split up by EFG into identical sites. Applying different field orientations causes different responses of the apical and in-plane sites (Fig. 5). In this way one can distinguish between them. The difference between the inner-apical O(1) and the outer-apical O(2) sites appears in the spectral intensities as the correspond-

ing composition ratio 1 : 2, as long as the spectrum is taken under the condition that the relaxation effects are small. Thus, the three sites in $Sr_3Ru_2O_7$ can be resolved from the complicated spectra shown in Fig. 3.

As displayed in Figs. 3 and 5, the impurity eutectic phase of Sr_2RuO_4 sometimes appears in NMR spectra, although the fraction of Sr_2RuO_4 in the powder X-ray diffraction spectra of our samples does not exceed a few percent. This is possible if during the annealing process the substitution of the oxygen atoms in the minor Sr_2RuO_4 part for ^{17}O is easier than the substitution in the $Sr_3Ru_2O_7$ part of the sample. The spectra positions and longitudinal relaxation rates $1/T_1$ of Sr_2RuO_4 are known[21], and hence, line crossing between $Sr_3Ru_2O_7$ and Sr_2RuO_4 can be avoided when measuring Knight shifts or $1/T_1$ of $Sr_3Ru_2O_7$.

B. Quadrupole splitting

The EFG at the oxygen site is the sum of the fields created by external ions and by on-site unclosed $2p$ shells. The former is largely enhanced over the value obtained by point-charge calculations due to polarization of the on-site closed shells. We employ the Sternheimer equation[22,23] to describe the EFG frequencies $^{17}\nu^i$:

$$^{17}\nu^i = (1-\gamma_\infty)\,^{17}\nu^i_{\rm lat} + (1-R)\,^{17}\nu^i_{\rm hole}, \qquad (2)$$

where $^{17}\nu^i_{\rm lat}$ is obtained from the EFG frequency of the point-charge calculation, and $^{17}\nu^i_{\rm hole}$ is that of the holes in the $2p$ orbitals. The two Sternheimer parameters γ_∞ and R are the antishielding and the shielding factors, respectively. R is approximately 0.1 for oxygen $2p$,[22,23] and we adopt this value. It is difficult to estimate the value of γ_∞ for O^{2-}. ^{17}O-NMR experiments in cuprates yielded γ_∞ of -8 (Ref. 24) or -9 (Ref. 25). However, theoretical calculations suggested a wide variety of values between -9 and -33,[26] indicating that the value is highly dependent on the ionic radius or covalency.[23]

Table I shows the measured EFG frequencies $^{17}\nu^i$ determined from the quadrupole splitting of the satellite lines and $^{17}\nu^i_{\rm lat}$ from calculations based on the point-charge model without considering holes at the oxygen sites. In the calculation, ions within at least three lattice units have to be included to obtain sufficient convergence. The spectral EFG frequencies do not feature any significant H and T (< 100 K) dependence, suggesting that the electronic band structure of $Sr_3Ru_2O_7$ is not strongly modified by the first-order metamagnetic transition. In fact, de Haas-van Alphen[30] and Shubnikov-de Haas[16] measurements revealed that the changes in the oscillating frequencies are quite small, supporting a field-induced Stoner transition model of the itinerant metamagnetism of $Sr_3Ru_2O_7$.

In the metallic ruthenate, the Fermi level is located between the bonding and the antibonding molecular orbitals,[14] and hence, the atomic $2p$ orbitals acquire holes. In terms of the hole occupancy h_{2p} of the $2p$ orbital, the induced EFG $^{17}\nu^i_{\rm hole}$ can be written as:

$$\begin{pmatrix} ^{17}\nu^x_{\rm hole} \\ ^{17}\nu^y_{\rm hole} \\ ^{17}\nu^z_{\rm hole} \end{pmatrix} = \frac{2}{5} e h_{2p} \left\langle r^{-3} \right\rangle_{2p} \begin{pmatrix} -1 \\ -1 \\ 2 \end{pmatrix}, \qquad (3)$$

for the $2p_z$ orbital, for instance. Taking $\left\langle r^{-3} \right\rangle_{2p}$ to be 3.63 a.u., which is a 70% value of that for a free atom,[25,35] $^{17}\nu^i_{\rm hole} = h_{2p}(-1.33, -1.33, 2.66)$ MHz. Thus, the total EFG frequency at each site is

(For the apical sites)

$$\begin{pmatrix} ^{17}\nu^{a,b} \\ ^{17}\nu^{c} \end{pmatrix} = (1-\gamma_\infty)\,^{17}\nu^i_{\rm lat} + (1-R) h_{2p_{a,b}} \begin{pmatrix} 1.33 \text{ MHz} \\ -2.66 \text{ MHz} \end{pmatrix}, \qquad (4)$$

(or for the in-plane sites)

$$\begin{pmatrix} ^{17}\nu^{\parallel} \\ ^{17}\nu^{\perp} \\ ^{17}\nu^{c} \end{pmatrix} = (1-\gamma_\infty)\,^{17}\nu^i_{\rm lat} + (1-R) h_{2p_c} \begin{pmatrix} -1.33 \text{ MHz} \\ -1.33 \text{ MHz} \\ 2.66 \text{ MHz} \end{pmatrix} + (1-R) h_{2p_{a,b}} \begin{pmatrix} -1.33 \text{ MHz} \\ 2.66 \text{ MHz} \\ -1.33 \text{ MHz} \end{pmatrix}. \qquad (5)$$

The antishielding factor γ_∞ cannot be solved from the above equations because of the dipole-field requirement $\sum_i {}^{17}\nu^i = 0$. Table II shows the hole occupancy in each orbital estimated from various values for γ_∞ and from band-structure calculations in literature. In this analysis, $\gamma_\infty < -8$ is necessary to make all densities positive. In the following we adopt the same value used in the case of the cuprates $\gamma_\infty = -9$[23,25]. This leads to a physically reasonable set of values for h_{2p}.

It should be noted that most of the holes reside at the in-plane sites (O(3) for $Sr_3Ru_2O_7$ and O(1) for Sr_2RuO_4), reflecting their quasi-two dimensionality. The large magnitude of the in-plane hole occupancy is in agreement with the strongly anisotropic conductivity ($\rho_c/\rho_{ab} \simeq 300$ for $Sr_3Ru_2O_7$[6] and $\gtrsim 400$ fo Sr_2RuO_4[2]) and with spin densities derived from the Knight shift measurements, which are discussed later.

Another remark concerns the relationship between hole occupancy and bonding covalency. In general, a hole in an antibonding molecular orbital introduces covalent character in the original ionic bond. Since a covalent bonding is sensitive to the Ru-O-Ru angle, the covalency can be related to a structural instability of the RuO_6 octahedra. In Sr_2RuO_4, Oguchi argued that the high h_{2p_c} in the $4d_{zx,yz}$-$2p_c$ (one of p_π) antibonding orbitals may account for an absence of a rotation of the RuO_6 octahedra.[14] Indeed, in Table II, h_{2p_c}, which is hybridized with $d_{zx,yz}$, has a larger value ($= 0.301$) than $h_{2p_{a,b}}$ ($= 0.202$) hybridizing with d_{xy} at the in-plane sites. In addition, a smaller value of h_{2p_c} ($= 0.256$) at the in-plane site is obtained for $Sr_3Ru_2O_7$, where the RuO_6 octahedra are rotated by 7°.[17] We consider that the existence of the rotation in $Sr_3Ru_2O_7$ is related to a weaker

TABLE I: Electric field gradients' (EFG) frequencies of the ruthenates determined from the observed electric quadrupole splittings, compared with those obtained from point-charge model calculations where the charges of the oxygen and the ruthenium are -2 and +4, respectively. The signs have been adjusted to obtain positive EFG frequencies along the principal axes. Order-of-magnitude differences between experimentally determined EFGs and calculated EFGs mostly arise from an antishielding effect $(1-\gamma_\infty)$. Lattice parameters used for the calculations are based on Refs. 17, 27, and 18 for $Sr_3Ru_2O_7$, Sr_2RuO_4, and $SrRuO_3$, respectively.

	$^{17}\nu^{\parallel,a}$ MHz	$^{17}\nu^{\perp,b}$ MHz	$^{17}\nu^{c}$ MHz	η	$^{17}\nu^{\parallel,a}_{\rm lat}$ MHz	$^{17}\nu^{\perp,b}_{\rm lat}$ MHz	$^{17}\nu^{c}_{\rm lat}$ MHz	$\eta_{\rm lat}$
				$Sr_3Ru_2O_7$				
O(1)	$\mp$0.47	$\mp$0.47	$\pm$0.94	0	-0.0830	-0.0830	0.1660	0
O(2)	$\mp$0.33	$\mp$0.33	$\pm$0.66	0	-0.0456	-0.0456	0.0910	0
O(3)	$\pm$0.78	$\mp$0.44	$\mp$0.34	0.11	0.1951	-0.0971	-0.0980	0.004
				Sr_2RuO_4				
O(1)	$\pm$0.77[a]	$\mp$0.45[a]	$\mp$0.32[a]	0.17[a]	0.2062	-0.0986	-0.1064	0.04
O(2)	$\mp$0.305[a]	$\mp$0.305[a]	$\pm$0.610[a]	0[a]	-0.0437	-0.0437	0.0874	0
				Paramagnetic $SrRuO_3$				
O	$\pm$0.95[b]				0.1782	-0.0891	-0.0891	0

[a] H. Murakawa *et al.*, single crystal with an accurate sample alignment in Ref. 28. Values are the same in Ref. 21 within errors.
[b] K. Yoshimura *et al.*, powder sample in Ref. 29.

TABLE II: Hole occupancies in the oxygen $2p$ orbitals obtained from the EFG analysis. Although the derivation of a reliable value of the Sternheimer antishielding factor γ_∞ is technically difficult, we argue that $\gamma_\infty = -9$ yields physically reasonable results (see text). $h_{2p}^{\rm total}$ denotes the total hole number per ruthenium atom. The given literature values of band-structure calculations have been estimated by integrating the DOS above $E_{\rm F}$.

	NMR EFG Analysis γ_∞			Band Calc.
	-8	-9	-10	
		$Sr_3Ru_2O_7$		
$h_{2p_{a,b}}^{\rm O(1)}$	0.056	0.075	0.092	
$h_{2p_{a,b}}^{\rm O(2)}$	0.005	0.009	0.021	
$h_{2p_{a,b}}^{\rm O(3)}$	0.178	0.199	0.218	
$h_{2p_c}^{\rm O(3)}$	0.232	0.256	0.277	
$h_{2p}^{\rm O(3)}$	0.410	0.455	0.495	0.28[a]
$h_{2p}^{\rm total}$	0.866	1.00	1.12	0.76[a]
		Sr_2RuO_4		
$h_{2p_{a,b}}^{\rm O(1)}$	0.183	0.202	0.219	
$h_{2p_c}^{\rm O(1)}$	0.276	0.301	0.323	
$h_{2p}^{\rm O(1)}$	0.459	0.503	0.542	0.27[b] 0.28[c]
$h_{2p_{a,b}}^{\rm O(2)}$	-0.001	0.012	0.023	
$h_{2p}^{\rm O(2)}$	-0.002	0.024	0.046	0.15[b] 0.09[c]
$h_{2p}^{\rm total}$	0.915	1.05	1.18	0.84[b] 0.75[c]
		Paramagnetic $SrRuO_3$		
$h_{2p}^{\rm O}$	0.120	0.143	0.164	
$h_{2p}^{\rm total}$	0.718	0.859	0.984	

[a] After Fig. 4 in Ref. 31.
[b] After Fig. 3 in Ref. 14.
[c] After Fig. 4 in Ref. 32.

covalency in the $d_{zx,yz}$-$2p_c$ bond than that in Sr_2RuO_4. For comparison with $SrRuO_3$, which has an octahedra tilt, the hole occupancy per ruthenium atom $h_{2p}^{\rm total}$ can be used. $SrRuO_3$ has the smallest value of $h_{2p}^{\rm total}$ in Table II, which means the weakest covalency per ruthenium atom. This might be related to the occurrence of the tilt in $SrRuO_3$ as well as the rotation in $Sr_3Ru_2O_7$.

We point out experimentally that the hole content of the antibonding orbitals may be substantially relevant to the distortion of the RuO_6 octahedra even in $Sr_{n+1}Ru_nO_{3n+1}$ which have the same tolerance factor.

C. Knight shift

Generally, the observed Knight shift $^{17}K_{\rm obs}$ (or the uniform susceptibility $\chi_{\rm bulk}$) for a given field direction $i\,(=x,y,z)$ is the sum of the temperature independent orbital part $^{17}K^i_{\rm orb}$ ($\chi^i_{\rm bulk,orb}$), the diamagnetic part $^{17}K^i_{\rm dia}$ ($\chi_{\rm bulk,dia}$), and the temperature dependent spin part $^{17}K^i_{\rm s}$ ($\chi^i_{\rm bulk,s}$), and are expressed as follows:

$$^{17}K^i_{\rm obs}(T) = {}^{17}K^i_{\rm orb} + {}^{17}K^i_{\rm dia} + {}^{17}K^i_{\rm s}(T), \quad (6)$$

$$\chi^i_{\rm bulk}(T) = \chi^i_{\rm bulk,orb} + \chi_{\rm bulk,dia} + \chi^i_{\rm bulk,s}(T), \quad (7)$$

$$^{17}K^i_{\rm s}(T) = \frac{^{17}A^i_{\rm s}}{N_{\rm A}\mu_{\rm B}}\chi^i_{\rm s}(T). \quad (8)$$

Here, $N_{\rm A}$, $\mu_{\rm B}$, and $^{17}A^i_{\rm s}$ denote Avogadro's number, the Bohr magneton, and the spin hyperfine coupling constant, respectively. Note that the spin part of $M/H_{\rm res}$ must be used instead of the differential susceptibility $\chi_{\rm bulk,s}$ in eq. (8) unless M is proportional to H.

Figure 6 shows a $^{17}K_{\rm obs}$ vs $M/H_{\rm res}$ plot of $Sr_3Ru_2O_7$. $^{17}K_{\rm obs}$ and $M/H_{\rm res}$ are measured at $\sim$ 4 T by changing temperature in a range of 1.7-100 K passing through

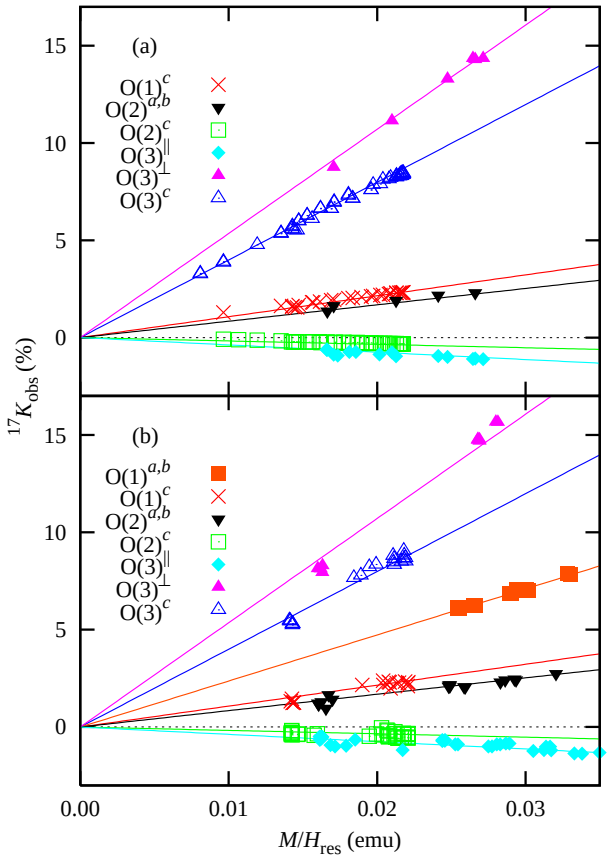

FIG. 6: (color online). $^{17}K_{\rm obs}$ vs $M/H_{\rm res}$ plots for $Sr_3Ru_2O_7$. The fitted hyperfine coupling constant for each curve is listed in Table III. (a) Temperature varied data points between 1.7 K and 100 K at low field $\simeq$ 4 T and (b) field varied points between 3 T and 13 T at 1.7 K. Below 7 T M is measured with a commercial SQUID magnetometer. For higher fields, M is interpolated (7 T – 8 T), derived from 2.8 K data given in Ref. 8 (8 T – 11 T), and extrapolated (> 11 T).

the susceptibility maximum at 16 K (Fig. 6(a)) and at 1.7 K by changing the magnetic field in a range of 3-13 T across the metamagnetic field (Fig. 6(b)). For the [100] direction, the temperature dependence for the O(1) site could not be measured due to the crossing of the lines to other sites. Linear relations are obtained in both cases and the solid lines are linear fits. The slopes of the K vs $M/H_{\rm res}$ plots for those two sets of data give the same hyperfine coupling constant $^{17}A^i_{\rm s}$. The orbital component of the Knight shifts are negligibly small since the lines intersect the origin. The obtained spin hyperfine coupling constants $^{17}A^i_{\rm s}$ are listed in Table III.

We extended the previous tight-binding approach[33] by including the magnetic dipolar fields from neighboring sites:

$$^{17}K^i_{\rm obs} = {}^{17}K^i_{\rm off-site} + {}^{17}K^i_{\rm on-site}. \quad (9)$$

The first term denotes the shift of the field produced by the moment of the adjacent sites, mostly of the nearest-neighbor ruthenium sites, and the second term is produced by the transferred spin densities in the oxygen on-site orbitals. In our case, the latter plays a major role as a result of a large local spin density.

The off-site part at the oxygen n site is written in terms of local susceptibilities at neighboring m sites χ^i_m:

$$\begin{aligned}
^{17}K^i_{\rm off-site,orb} &= \frac{1}{N_{\rm A}\mu_{\rm B}} \sum_{m(\neq n)} \frac{\partial^2}{\partial i^2}\left(\frac{1}{r_{mn}}\right)\chi^i_{m,\rm orb},\\
^{17}K^i_{\rm off-site,dia} &= \frac{1}{N_{\rm A}\mu_{\rm B}} \sum_{m(\neq n)} \frac{\partial^2}{\partial i^2}\left(\frac{1}{r_{mn}}\right)\chi_{m,\rm dia},\\
^{17}K^i_{\rm off-site,s}(T) &= \frac{1}{N_{\rm A}\mu_{\rm B}} \sum_{m(\neq n)} \frac{\partial^2}{\partial i^2}\left(\frac{1}{r_{mn}}\right)\chi^i_{m,\rm s}(T).
\end{aligned} \quad (10)$$

Here, r_{mn} is the distance between two sites m and n. The summations are taken over a distance of four lattice units to ensure convergence. Since $\chi_{\rm bulk,s}$ of $Sr_3Ru_2O_7$ and $SrRuO_3$ are strongly enhanced ($> 1\times10^{-2}$ emu/Ru-mol), the orbital part or diamagnetic part of χ (typically 10^{-4} emu/Ru-mol[33]) for those compounds can be neglected. For Sr_2RuO_4, the estimated values of $^{17}K_{\rm orb} + {}^{17}K_{\rm dia}$ are also given in Table III. For all three compounds, the off-site hyperfine coupling constants from the ruthenium sites to the oxygen sites $|\sum_{m=\rm Ru}\frac{\partial^2}{\partial i^2}(\frac{1}{r_{mn}})|$ is small ($<$ 5 kOe/$\mu_{\rm B}$). Therefore, the ^{17}O Knight shifts are dominated by the on-site spin parts, which we will discuss next.

Assuming that only the ruthenium orbitals contribute to the orbital part of the bulk susceptibility, the on-site Knight shifts at the oxygen sites arise solely from the spin part,

$$^{17}K^i_{\rm on-site}(T) = \sum_{k=\{2p_{a,b,c},2s\}} \frac{^{17}A^i_k}{N_{\rm A}\mu_{\rm B}}\chi^i_{k,\rm s}(T), \quad (11)$$

where $^{17}A^i_k$ is the hyperfine coupling constant and $\chi^i_{k,\rm s}(T)$ is the transferred spin density, and the subscript $k\,(=2p, 2s)$ specifies the orbital. Since the isotropic hyperfine coupling of the $2s$ orbital $^{17}A_{2s}$ is quite large due to its Fermi contact to the nucleus ($^{17}A_{2s} \sim 3000$ kOe/$\mu_{\rm B}$[34]), isotropic shifts still dominate even with a tiny spin density in the $2s$ orbitals. The hyperfine couplings of $2p$ orbitals have an anisotropic dipole character, $2\,^{17}A_{2p}(-1,-1,2)$ for each $2p$ orbital, where $^{17}A_{2p} = \frac{2}{5}\mu_{\rm B}\langle r^{-3}\rangle_{2p} \simeq 91$ kOe/$\mu_{\rm B}$.[25,35]

Next, we assume that the ratios of transferred orbital spin densities $\chi_{k,s}/\chi_{\rm bulk,s}$ $(k = 2p, 2s)$ are independent of the field orientation even in the case of anisotropic spin susceptibilities. Non-bonding $2p_\sigma$ orbitals can be ignored because states arising from those orbitals are much below $E_{\rm F}$. Thus, the total on-site hyperfine coupling constant $^{17}A_{\rm s,on-site}$ for each field orientation is simplified to:

TABLE III: ^{17}O Hyperfine coupling constants $^{17}A_{\rm s}$. $^{17}A_{\rm s}$ of $Sr_3Ru_2O_7$ are obtained from fittings of $^{17}K_{\rm obs}$ vs $M/H_{\rm res}$ plots (Fig. 6). Estimated non-spin parts of the Knight shifts $^{17}K_{\rm orb}$ + $^{17}K_{\rm dia}$ for Sr_2RuO_4 are also shown. For the other compounds, the non-spin parts are negligibly small.

	$^{17}A_{\rm s}$ (kOe/$\mu_{\rm B}$)	$^{17}K_{\rm orb}$ + $^{17}K_{\rm dia}$ (%)
	$Sr_3Ru_2O_7$	
O(1)^{a,b}	13.2 ± 0.2	
O(1)^{c}	6.0 ± 0.2	
O(2)^{a,b}	4.7 ± 0.3	
O(2)^{c}	-0.97 ± 0.05	
O(3)$^{\parallel}$	-2.1 ± 0.3	
O(3)$^{\perp}$	29.9 ± 0.3	
O(3)^{c}	22.3 ± 0.4	
	Sr_2RuO_4	
O(1)$^{\parallel}$	-7.9 ± 1^{a}	0.013
O(1)$^{\perp}$	33.1 ± 1^{a}	-0.006
O(1)^{c}	23.7 ± 1^{a}	-0.005
O(2)^{a,b}	6.4 ± 1^{a}	-0.003
O(2)^{c}	1.9 ± 1^{a}	0.004
	Paramagnetic $SrRuO_3$	
O$^{\parallel}$	6.3 ± 2^{b}	
O$^{\perp}$	21 ± 2^{b}	

[a] H. Murakawa *et al.*, single crystal with an accurate sample alignment in Ref. 28. Knight shifts are taken below 4 K and are the same in Ref. 33 within errors.

[b] Anisotropic Knight shifts are estimated from the powder patterns above $T_{\rm C}$ by pattern simulations. The spectra used in the study of Ref. 29 were provided by Yoshimura *et al.*

(For the apical sites)

$$\begin{pmatrix} ^{17}A^{a,b}_{\rm s,on-site} \\ ^{17}A^{c}_{\rm s,on-site} \end{pmatrix} = \begin{pmatrix} 1 & 1 \\ -2 & 1 \end{pmatrix} \begin{pmatrix} 2\,^{17}A_{2p}\chi_{2p_{x,y},\rm s}/\chi_{\rm bulk,s} \\ ^{17}A_{2s}\chi_{2s,\rm s}/\chi_{\rm bulk,s} \end{pmatrix}, \tag{12}$$

(or for the in-plane sites)

$$\begin{pmatrix} ^{17}A^{\parallel}_{\rm s,on-site} \\ ^{17}A^{\perp}_{\rm s,on-site} \\ ^{17}A^{c}_{\rm s,on-site} \end{pmatrix} = \begin{pmatrix} -1 & -1 & 1 \\ 2 & -1 & 1 \\ -1 & 2 & 1 \end{pmatrix} \begin{pmatrix} 2\,^{17}A_{2p}\chi_{2p_{x,y},\rm s}/\chi_{\rm bulk,s} \\ 2\,^{17}A_{2p}\chi_{2p_{c},\rm s}/\chi_{\rm bulk,s} \\ ^{17}A_{2s}\chi_{2s,\rm s}/\chi_{\rm bulk,s}. \end{pmatrix}, \tag{13}$$

Since the spin density at strontium sites can be ignored, the bulk spin susceptibility $\chi_{\rm bulk,s}$ is the sum of the spin densities in the oxygen and the ruthenium orbitals,

$$\chi_{\rm bulk,s} = \chi^{\rm Ru}_{\rm s} + \chi^{\rm total}_{2p,\rm s} + \chi^{\rm total}_{2s,\rm s}. \tag{14}$$

For $Sr_3Ru_2O_7$, the total spin densities over all oxygen sites per ruthenium atom $\chi^{\rm total}_{2p,\rm s}$ and $\chi^{\rm total}_{2s,\rm s}$ are:

$$\chi^{\rm total}_{2p,\rm s} = \chi^{\rm O(1)}_{2p_{a,b},\rm s} + 2\chi^{\rm O(2)}_{2p_{a,b},\rm s} + 2\chi^{\rm O(3)}_{2p_{a,b},\rm s} + 2\chi^{\rm O(3)}_{2p_{c},\rm s}, \tag{15}$$

$$\chi^{\rm total}_{2s,\rm s} = \frac{1}{2}\chi^{\rm O(1)}_{2s,\rm s} + \chi^{\rm O(2)}_{2s,\rm s} + 2\chi^{\rm O(3)}_{2s,\rm s}. \tag{16}$$

TABLE IV: Orbital spin densities obtained from Knight-shift measurements and the density of states at the Fermi level $D(E_{\rm F})$ at the oxygen site extracted from the results of band-structure calculations. Spin densities and $D(E_{\rm F})$ are normalized by the bulk spin susceptibility per ruthenium atom $\chi_{\rm bulk,s}$.

	χ(per orb.)/$\chi_{\rm bulk,s}$ %	χ(per Ru)/$\chi_{\rm bulk,s}$ %	$D(E_{\rm F})$ %
	$Sr_3Ru_2O_7$		
$\chi^{\rm O(1)}_{2p_{a,b},\rm s}$	1.71 ± 0.06	1.71 ± 0.06	3^{a}
$\chi^{\rm O(1)}_{2s,\rm s}$	0.360 ± 0.005	0.180 ± 0.003	
$\chi^{\rm O(2)}_{2p_{a,b},\rm s}$	1.50 ± 0.06	3.00 ± 0.11	2^{a}
$\chi^{\rm O(2)}_{2s,\rm s}$	0.093 ± 0.007	0.093 ± 0.007	
$\chi^{\rm O(3)}_{2p_{a,b},\rm s}$	6.38 ± 0.08	12.8 ± 0.16	
$\chi^{\rm O(3)}_{2p_{c},\rm s}$	5.03 ± 0.09	10.1 ± 0.18	
$\chi^{\rm O(3)}_{2p,\rm s}$		22.9 ± 0.3	20^{a} 21^{b}
$\chi^{\rm O(3)}_{2s,\rm s}$	0.557 ± 0.007	1.113 ± 0.013	
$\chi^{\rm total}_{2p,\rm s}$		27.5 ± 0.3	25^{a} 25^{b}
$\chi^{\rm total}_{2s,\rm s}$		1.39 ± 0.015	
	Sr_2RuO_4		
$\chi^{\rm O(1)}_{2p_{a,b},\rm s}$	8.4 ± 0.24	16.7 ± 0.5	
$\chi^{\rm O(1)}_{2p_{c},\rm s}$	6.8 ± 0.23	13.6 ± 0.5	
$\chi^{\rm O(1)}_{2p,\rm s}$		30.3 ± 0.8	15^{c} 26^{d} 21^{e}
$\chi^{\rm O(1)}_{2s,\rm s}$	0.54 ± 0.02	1.11 ± 0.04	
$\chi^{\rm O(2)}_{2p_{a,b},\rm s}$	1.2 ± 0.24	5.0 ± 0.9	3^{c} 4^{d} 4^{e}
$\chi^{\rm O(2)}_{2s,\rm s}$	0.16 ± 0.024	0.33 ± 0.05	
$\chi^{\rm total}_{2p,\rm s}$		35.3 ± 1.2	18^{c} 29^{d} 25^{e}
$\chi^{\rm total}_{2s,\rm s}$		1.41 ± 0.06	
	Paramagnetic $SrRuO_3$		
$\chi^{\rm O}_{2p,\rm s}$	3.6 ± 0.5	22 ± 3	21^{f} 30^{g}
$\chi^{\rm O}_{2s,\rm s}$	0.54 ± 0.05	1.6 ± 0.15	

[a] Reference 36.
[b] FLAPW within LSDA. Taken from figures in Ref. 31.
[c] LAPW within LDA. Taken from Fig. 3 in Ref. 14.
[d] LAPW within LDA. Taken from Fig. 2 in Ref. 37.
[e] FLAPW within LSDA. Taken from figs in Ref. 32.
[f] LMTO within LSDA in Ref. 38.
[g] Approximate value in Ref. 39.

Thus, the observed anisotropic Knight shifts can be decomposed into the local spin density in each orbital from eqs. (6)-(16).

Table IV displays the local spin densities in the oxygen orbitals obtained from Knight shifts and the DOS at $E_{\rm F}$, $D(E_{\rm F})$ from band-structure calculations in literature. The spin density is generally enhanced over the value of $D(E_{\rm F})$ which comes out of band-structure calculations due to Stoner enhancement and untreated electron-electron correlations. The bulk susceptibility of $Sr_3Ru_2O_7$ is the product of the value inferred from the electronic specific heat and the large Wilson ratio 10 (Ref. 6). If such a Stoner enhancement varies between bands and/or site-by-site, the enhancement factors applied to local spin densities would differ from orbital to orbital. In Table IV, the normalized values of spin densities and of $D(E_{\rm F})$ are essentially comparable for each

oxygen site. The Stoner enhancement of these ruthenates appears to be independent of the orbitals.

According to this analysis, the total spin density at the oxygen sites amounts to 20-40% of the bulk susceptibility. This is quite large for a metallic oxide. Indeed, a polarized neutron scattering study on the exchange enhanced paramagnet $Ca_{1.5}Sr_{0.5}RuO_4$ by A. Gukasov and co-workers (Ref. 40) revealed that the in-plane site O(1) and the apical site O(2) have 30% and 4% of the total moment, respectively, and the totaling one third of moments resides at the oxygen sites. In the case of Sr_2RuO_4 the values are similar to our results shown in Table IV.

It is found that higher dimensional members have a much smaller fraction of spin densities at the oxygen sites $\chi^{\rm total}_{2p,{\rm s}}/\chi_{\rm bulk,s}$, while the variation of the hole occupancies $h^{\rm total}_{2p}$ in Table II is small. Therefore, we can deduce that $SrRuO_3$ has a largely enhanced $D(E_{\rm F})$ especially at the ruthenium site because of the on-site Coulomb interactions at the ruthenium site. In a Stoner mechanism, the partially localized character of the 4*d* electrons and resulting narrow bands and high $D(E_{\rm F})$ are favorable for itinerant ferromagnetism and metamagnetism, as is systematically observed in 3*d* and 4*d* pure metals. The ferromagnetism of $SrRuO_3$ could be related to the smallness of the transferred spin density at the oxygen site.

In addition to the ferromagnetic fluctuations in $Sr_3Ru_2O_7$, incommensurate antiferromagnetic fluctuations were found,[13,41] which are similar to those in Sr_2RuO_4.[4] These incommensurate antiferromagnetic fluctuations arise from the Fermi-surface nesting of one-dimensional Fermi-surface sheets, when the small spin density at the apical oxygen site weakens the transfer between RuO_2 layers, resulting in the low-dimensional character. We thus clarified the important roles of hole occupation and spin density in different oxygen orbitals and their relevance for the ferromagnetic and antiferromagnetic character of the ruthenates $Sr_{n+1}Ru_nO_{3n+1}$.

IV. CONCLUSION

In conclusion, we have investigated microscopic hole occupancies and transferred spin densities at the oxygen sites by analyzing the ^{17}O-NMR electric field gradients and anisotropic Knight shifts of $Sr_{n+1}Ru_nO_{3n+1}$ ($n = 1, 2, \infty$). The hole occupancies at the oxygen sites are quite large, which is unexpected for a non-doped oxide. This gives evidence that the covalent character of the Ru-O bonding plays an important role in these compounds. The tilting ($SrRuO_3$) and the rotation ($Sr_3Ru_2O_7$) of the RuO_6 octahedra may account for a weaker covalency, which originates from insufficient holes in the p_π antibonding orbitals which is not the case in the undistorted Sr_2RuO_4.

The total spin densities at the oxygen sites derived from anisotropic ^{17}O-Knight shifts are also high (20-40% of the bulk spin susceptibility), which is, however, in good agreement with band-structure calculations and results obtained from polarized neutron experiments reported in literature. Although the total oxygen hole occupancies per ruthenium atom do not significantly change among the series $Sr_{n+1}Ru_nO_{3n+1}$, the spin densities at the oxygen sites decrease with increasing n. This suggests that higher dimensional members of the series have narrower bands and, as a result, metamagnetism and itinerant ferromagnetism are induced in $Sr_3Ru_2O_7$ and $SrRuO_3$, respectively. It is shown that the enhancement of the spin density at the oxygen site is comparable with that at the ruthenium site. The spin density at the apical oxygen site (O(2) in Sr_2RuO_4, O(1) and O(2) in $Sr_3Ru_2O_7$) is much smaller than that at the in-plane oxygen site, which is responsible for the strong two-dimensional character in those compounds. The low dimensionality might lead to the occurrence of one-dimensional Fermi-surface nesting. This would explain the incommensurate antiferromagnetic fluctuations, which emerge in Sr_2RuO_4 and in $Sr_3Ru_2O_7$. Structural distortions and magnetism in $Sr_{n+1}Ru_nO_{3n+1}$ are strongly related with the covalent character of the Ru 4*d*-O 2*p* molecular orbitals and the spin densities at the oxygen sites.

Acknowledgments

We thank H. Yaguchi, M. Kriener, E. M. Forgan, and H. Ikeda for stimulating discussions and comments. This work was in part supported by the Grants-in-Aid for Scientific Research from JSPS and MEXT of Japan and by the 21COE program "Center for Diversity and Universality in Physics" from MEXT of Japan.

* Electronic address: kitagawa@scphys.kyoto-u.ac.jp

[1] Y. Maeno, H. Hashimoto, K. Yoshida, S. Nishizaki, T. Fujita, J. G. Bednorz, and F. Lichtenberg, Nature **372**, 532 (1994).
[2] A. P. Mackenzie and Y. Maeno, Rev. Mod. Phys. **75**, 657 (2003).
[3] K. Ishida, H. Mukuda, Y. Kitaoka, K. Asayama, Z. Q. Mao, Y. Mori, and Y. Maeno, Nature **396**, 658 (1998).
[4] Y. Sidis, M. Braden, P. Bourges, B. Hennion, S. NishiZaki, Y. Maeno, and Y. Mori, Phys. Rev. Lett. **83**, 3320 (1999).
[5] J. M. Longo, P. M. Raccah, and J. B. Goodenough, J. App. Phys. **39**, 1327 (1968).
[6] S. I. Ikeda, Y. Maeno, S. Nakatsuji, M. Kosaka, and Y. Uwatoko, Phys. Rev. B **62**, R6089 (2000).
[7] S. Ikeda, N. Shirakawa, T. Yanagisawa, Y. Yoshida, S. Koikegami, S. Koike, M. Kosaka, and Y. Uwatoko, J. Phys. Soc. Jpn. **73**, 1322 (2004).
[8] R. S. Perry, L. M. Galvin, S. A. Grigera, L. Capogna, A. J. Schofield, A. P. Mackenzie, M. Chiao, S. R. Julian, S. Ikeda, S. Nakatsuji, et al., Phys. Rev. Lett. **86**, 2661

(2001).
[9] R. S. Perry, T. Tayama, K. Kitagawa, T. Sakakibara, K. Ishida, and Y. Maeno, J. Phys. Soc. Jpn. **74**, 1270 (2005).
[10] S. A. Grigera, R. A. Borzi, A. P. Mackenzie, S. R. Julian, R. S. Perry, and Y. Maeno, Phys. Rev. B **67**, 214427 (2003).
[11] A. J. Millis, A. J. Schofield, G. G. Lonzarich, and S. A. Grigera, Phys. Rev. Lett. **88**, 217204 (2002).
[12] S. A. Grigera, R. S. Perry, A. J. Schofield, M. Chiao, S. R. Julian, G. G. Lonzarich, S. I. Ikeda, Y. Maeno, A. J. Millis, and A. P. Mackenzie, Science **294**, 329 (2001).
[13] K. Kitagawa, K. Ishida, R. S. Perry, T. Tayama, T. Sakakibara, and Y. Maeno, Phys. Rev. Lett. **95**, 127001 (2005).
[14] T. Oguchi, Phys. Rev. B **51**, 1385 (1995).
[15] R. S. Perry and Y. Maeno, J. Crystal Growth **271**, 134 (2004).
[16] R. S. Perry, K. Kitagawa, S. A. Grigera, R. A. Borzi, A. P. Mackenzie, K. Ishida, and Y. Maeno, Phys. Rev. Lett. **92**, 166602 (2004).
[17] H. Shaked, J. D. Jorgensen, S. Short, O. Chmaissem, S. I. Ikeda, and Y. Maeno, Phys. Rev. B **62**, 8725 (2000).
[18] C. W. Jones, P. D. Battle, P. Lightfoot, and W. T. Harrison, Acta Cryst. **C45**, 365 (1989).
[19] G. C. Carter, L. H. Bennett, and D. J. Kahan, *Metallic Shifts in NMR* (Pergamon Press, Oxford, 1977).
[20] K. Kitagawa, K. Ishida, R. S. Perry, and Y. Maeno, Physica B **378-380C**, 119 (2006).
[21] H. Mukuda, K. Ishida, Y. Kitaoka, K. Asayama, and Z. Q. Mao, J. Phys. Soc. Jpn. **67**, 3945 (1998).
[22] R. Stermheimer, Phys. Rev. **84**, 244 (1951).
[23] E. P. Stoll, P. F. Meier, and T. A. Claxton, Phys. Rev. B **65**, 064532 (2002).
[24] K. R. Thurber, A. W. Hunt, T. Imai, F. C. Chou, and Y. S. Lee, Phys. Rev. Lett. **79**, 171 (1997).
[25] M. Takigawa, P. C. Hammel, R. H. Heffner, Z. Fisk, K. C. Ott, and J. D. Thompson, Phys. Rev. Lett. **63**, 1865 (1989).
[26] K. D. Sen and P. T. Narasimhan, Phys. Rev. B **15**, 95 (1977), and references therein.
[27] O. Chmaissem, J. D. Jorgensen, H. Shaked, S. Ikeda, and Y. Maeno, Phys. Rev. B **57**, 5067 (1998).
[28] H. Murakawa, K. Kitagawa, K. Ishida, and Y. Maeno, unpublished.
[29] K. Yoshimura, T. Imai, T. Kiyama, K. R. Thurber, A. W. Hunt, and K. Kosuge, Phys. Rev. Lett. **83**, 4397 (1999).
[30] R. A. Borzi, S. A. Grigera, R. S. Perry, N. Kikugawa, K. Kitagawa, Y. Maeno, and A. P. Mackenzie, Phys. Rev. Lett. **92**, 216403 (2004).
[31] I. Hase and Y. Nishihara, J. Phys. Soc. Jpn. **66**, 3517 (1997).
[32] I. Hase and Y. Nishihara, J. Phys. Soc. Jpn. **65**, 3957 (1996).
[33] T. Imai, A. W. Hunt, K. R. Thurber, and F. C. Chou, Phys. Rev. Lett. **81**, 3006 (1998).
[34] M. Takigawa, in *Proceedings of the NATO Advanced Research Workshop on Dynamics of Magnetic Fluctuations in High Temperature Superconductors* (Plenum, New York, 1990).
[35] J. S. M. Harvey, Proc. Roy. Soc. London A **285**, 581 (1965).
[36] D. J. Singh and I. I. Mazin, Phys. Rev. B **63**, 165101 (2001).
[37] D. J. Singh, Phys. Rev. B **52**, 1358 (1995).
[38] P. B. Allen, H. Berger, O. Chauvet, L. Forro, T. Jarlborg, A. Junod, B. Revaz, and G. Santi, Phys. Rev. B **53**, 4393 (1996).
[39] I. I. Mazin and D. J. Singh, Phys. Rev. B **56**, 2556 (1997).
[40] A. Gukasov, M. Braden, R. J. Papoular, S. Nakatsuji, and Y. Maeno, Phys. Rev. Lett. **89**, 087202 (2002).
[41] L. Capogna, E. M. Forgan, S. M. Hayden, A. Wildes, J. A. Duffy, A. P. Mackenzie, R. S. Perry, S. Ikeda, Y. Maeno, and S. P. Brown, Phys. Rev. B **67**, 012504 (2003).
[42] Equation (1) only contains the first order term with regard to the perturbations from EFG. For quantitative analyses, the second order perturbations must be included.